Journal of Luminescence 188 (2017) 514–523

Contents lists available at ScienceDirect

Journal of Luminescence

journal homepage: www.elsevier.com/locate/jlumin

Tunnelling recombination in conventional, post-infrared and post-infrared multi-elevated temperature IRSL signals in microcline K-feldspar

Eren Şahiner[a,b,*], George Kitis[b], Vasilis Pagonis[c], Niyazi Meriç[a], George S. Polymeris[a]

[a] Institute of Nuclear Sciences, Ankara University, Beşevler 06100, Ankara, Turkey
[b] Aristotle University of Thessaloniki, Nuclear Physics Laboratory, 54124 Thessaloniki, Greece
[c] McDaniel College, Physics Department, Westminster, MD 21157, USA

ARTICLE INFO

Keywords:
Tunnelling recombination
pIRIR
MET-pIRIR
De-convolution
Thermal activation
Band tails

ABSTRACT

In this manuscript, we study three different types of infrared stimulated luminescence signals (IRSL) from a microcline K-feldspar. These signals consist of conventional infrared (IR) stimulation measured at elevated temperatures, multi-elevated temperature post-infrared IRSL signals (MET-pIRIR), and post-infrared IRSL (pIRIR) signals. All three types of signals were analysed using analytical expressions previously derived according to a model based on quantum tunnelling. For the purpose of identifying various tunnelling components, de-convolution analysis was used based on continuous wave infrared stimulation (CW-IRSL), as well as de-convolution based on pseudo linearly modulated transformation of the signals (pLM-IRSL). The variation of the parameters with stimulation temperature was determined using both of these de-convolution methods of analysis. The luminescence curves and normalized signals were investigated at various temperatures using several related protocols. The results of this analysis have implications for the understanding of the emission of luminescence in this material during the above-mentioned protocols, and they highlight the strengths and shortfalls of the tunnelling recombination models. The results from this study contribute to a better understanding of the origin of pIRIR and MET-pIRIR luminescence signals.

1. Introduction

Luminescence dating techniques have been effectively applied for various quaternary deposits and archaeological samples. Much effort has been put into developing new luminescence dating protocols, in order to extend the dateable age range and to overcome the well-known problem of anomalous fading of luminescence signals in minerals. Infrared stimulated luminescence (IRSL) in feldspars offers the potential to date further back in time, as it is generally reported to saturate at much higher doses [1,2], although this is often hampered by the problem of anomalous fading of the feldspar signal [3]. Overcoming this problem might be possible by determining the rate of fading, and using one of several models proposed for the correction of measured burial doses [4–6].

It was demonstrated that IRSL measurements at high temperatures could isolate a more stable luminescence signal [7]. Among the promising techniques to address these issues, post-IR IRSL dating (hereafter called pIRIR), being a two-step protocol that uses an IRSL signal from feldspar that is less affected by anomalous fading, stands as very promising. [8] have shown that fading of feldspars is dependent on the temperature at which the IRSL measurement takes place; moreover, the IRSL signal stimulated at an elevated temperature, following stimulation at 50 °C, yields significantly less fading, and they referred to this as a pIRIR signal. Later on, in order to overcome anomalous fading K-feldspars from sediments, [7] introduced a multi-step protocol, which includes post IR IRSL measurements at sequentially increasing temperatures. This later protocol was termed as multi-elevated-temperature post-IR IRSL (MET-pIRIR hereafter). Both these techniques have been tested extensively using different temperature combinations in various protocols [9–18].

[19] have studied the origin of the non-fading luminescence signal in feldspar using time-resolved optically stimulated luminescence (TR-OSL), TR-IRSL and TR-pIR IRSL. They discussed a model for feldspar luminescence in which there exists a continuum of transitions occurring by phonon-assisted diffusion (PAD). Recently, [20] have analysed kinetics of infrared stimulated luminescence in feldspars; they have also extended their previous localized transition model [21] to enable Arrhenius analysis, and to allow analysis of experimentally obtained IRSL decay curves that arise from truncated nearest-neighbour distributions. By analyzing the effect of optical and isothermal treatments

* Corresponding author at: Institute of Nuclear Sciences, Ankara University, Beşevler 06100, Ankara, Turkey.
E-mail address: sahiner@ankara.edu.tr (E. Şahiner).

http://dx.doi.org/10.1016/j.jlumin.2017.05.010
Received 19 December 2016; Received in revised form 2 May 2017; Accepted 3 May 2017
Available online 04 May 2017

on luminescence signals from feldspars, [22] have developed an alternative mathematical approach to the one suggested by [21]. Despite all this recent work, the connection between the crystal structure and the physical mechanism of luminescence production in feldspar samples currently stands as an open research topic.

Based on (a) the different behaviours of isothermal signals from several dosimetric materials, such as Durango apatite [23] and MgB_4O_7:Dy,Na [24], as well as (b) the IRSL signal of contaminated quartz [25], it was suggested by [24,26] that either isothermal TL or IRSL measurements at high temperatures could be used as a probe in order to distinguish the recombination pathways of luminescence signals. Specifically, these authors suggested that such studies can help distinguishing between phosphors whose luminescence signal production involves delocalized kinetics, or transitions based on localized recombination processes. The present study follows directly from this recent suggestion by these authors.

The primary aim of the present work is studying whether the three different modes of IRSL signal measured from a K-feldspar sample, namely conventional IRSL, MET-pIRIR and pIRIR can be effectively described by tunnelling recombination processes.

The specific goals of this study are:

(a) to analyze the IRSL signal decay curve shapes by using a component-resolved de-convolution analysis, based on the tunnelling model originally developed by [21], and further developed mathematically by [26],
(b) to discuss the experimental results within the framework of these tunnelling models,
(c) to provide a physical explanation for the fitting parameters obtained for the various tunnelling components and
(d) to compare the results of the present study to those reported previously in the literature.

2. Materials, methods and experimental protocols

The sample used for the present study consists of a naturally occurring pure K-feldspar microcline sample from igneous rocks of Northern Greece, with laboratory code name SAM2 [27]. The luminescence signals from this specific feldspar sample have been studied previously in [22,27,28] and [29]. These authors suggested that these samples are ideal for investigating basic TL, OSL and IRSL signals along with the possible correlations between them.

All luminescence measurements were carried out using a Risø TL/OSL reader (model TL/OSL-DA-20), equipped with a $^{90}Sr/^{90}Y$ beta particle source, delivering a nominal dose rate of 0.130 ± 0.004 Gy/s. A 9635QA photomultiplier tube was used for light detection. The stimulation for IRSL includes IR diodes, with a stimulation wavelength of 875 (± 40) nm and a maximum power of ~135 mW cm^{-2} [30,31]. The detection optics consisted of a combination of the 2 mm Schott BG 39 and the 4 mm Corning 7-59 (known as the blue filter pack).

In the present work a single, unique and compact protocol was implemented, which includes the following steps:

Step 1: Attribute test dose
Step 2: IRSL measurement at $T_i = 50$ °C (unique measurement),
Step 3: IRSL measurement at $T_j = 50$ °C (unique measurement),
Step 4: IRSL measurements at T_k sequentially increasing between T_j and 300 °C in steps of 25 °C (series of measurements),
Step 5: Residual TL measurement at 500 °C (heating rate 1 °C/s),
Step 6: Repeat steps 1–5 for sequentially increasing T_j in step 3, ranging between 75 and 300 °C in steps of 25 °C,
Step 7: Repeat steps 1–5 for a different T_i in step 2, ranging between 75 and 300 °C in steps of 25 °C.

As it becomes obvious, the aforementioned protocol includes a series of measurements of all three types of IRSL stimulation modes, namely (a) initial or conventional IRSL (at various temperatures) during step 2, (b) $pIRIR_{Ta,Tb}$ during step 3 and (c) multi elevated temperature IRSL (hereafter MET-$pIRIR_{Ta,Tb}$) during step 4. These different signals were measured in the entire temperature region between 50 °C and 300 °C, in order to check the temperature effect in the luminescence emission of IR stimulation. Although the protocol applied in the present work is not exactly the same as the protocols in the already published $pIRIR_{Ta,Tb}$ papers in the literature, it scans all temperatures combinations commonly used in $pIRIR_{Ta,Tb}$ applications. As far as notation is concerned, in all cases, the subscript T_a denotes the temperature of the initial (conventional) IRSL measurement. The meaning of T_b depends on the type of the measurement sequence; for the two step case of $pIRIR_{Ta,Tb}$, T_b denotes the temperature of the second IRSL measurement, while in all cases of MET-$pIRIR_{Ta,Tb}$ T_b denotes the final temperature of the multistep sequential IRSL measurement. Finally, when no indexes are included, MET-pIRIR takes place throughout the entire temperature region from room temperature to 300 °C. Since all IRSL measurements were performed at elevated temperatures, all heatings at the selected temperature before IRSL were performed in a nitrogen atmosphere with a low constant heating rate of 2 °C/s, in order to avoid significant temperature lag effects [32].

Step 5 measures the residual thermoluminescence signal (rTL), which is recorded in order to check the TL behaviour at various IR stimulation steps. In general, the final stimulation temperature in all cases of MET-pIRIR is always 300 °C. Since all rTL glow curves coincide, throughout the applied protocol, the rTL signal was also measured for some extra specific cases, including after (i) initial IRSL at each stimulation temperatures, namely rTL after the first unique IRSL measurement, (b) each $pIRIR_{50,Tb}$ measurement, namely rTL after the sequence of the first two IRSL measurements, among which the first is undertaken at 50 °C and (c) each MET-$pIRIR_{50,Tb}$, namely rTL after a series of IRSL measurements at temperatures sequentially increasing from 50 °C and upwards. The test dose attributed was 100 Gy and was attributed to the K-feldspar sample every time that a measurement sequence finishes, namely after each rTL measurement. TL measurements were performed in a nitrogen atmosphere with a low constant heating rate of 2 °C/s, in order to avoid significant temperature lag effects [32].

3. Analysis of the IRSL signals

The physical processes that generate luminescence in feldspars are quite complex, since their IRSL decay is not exponential [33]. [26] have quantified the semi analytical model of [21] by deriving easy to use analytical expressions for different experimental stimulation modes. De-convolution analysis of all IRSL signals was performed using these equations as:

$$I(t) = \frac{3n_0\rho' zF(t)^2}{1+z\frac{t}{\tau}} e^{-\rho' F(t)^3} \quad (1)$$

$$F(t) = ln\left(1 + z\frac{t}{\tau}\right) \quad (2)$$

$$\tau = (\sigma\cdot\varphi)^{-1} \quad (3)$$

I(t) is the luminescence intensity as a function of stimulation time *t*; n_o is the initial concentration of the donors; z is a constant; τ the tunnelling luminescence lifetime for recombination processes taking place via the excited state; ρ' is a dimensionless parameter representing the normalized donor–acceptor density; σ is the photo-ionization cross section and φ the stimulation flux.

The de-convolution analysis was performed in two different ways: (a) by performing a direct least squares fitting analysis to the decaying, although not exponential, continuous-wave (CW) IRSL and (b) by transforming these featureless curves into pseudo linearly modulated (hereafter pLM-IRSL) curves [34]. Transformations of conventionally

measured CW-IRSL curves into pLM curves were achieved by using the equations suggested by [35], introducing two new parameters, namely the total illumination time P and the transformed time parameter u. These new parameters are related to those of the conventional CW IRSL parameters according to the following equations:

$$P = 2 \cdot t_{max} \tag{4}$$

$$u = \sqrt{(2 \cdot t \cdot P)} \tag{5}$$

The new transformed luminescence intensity of the pLM-IRSL signal is then calculated according to:

$$I_{pLM} = I_{CW} \cdot \left(\frac{u}{P}\right) \tag{6}$$

where I_{CW} stands for the intensity of the continuous wave IRSL measurement. All curve fittings were performed using the software package Microsoft Excel, with the Solver utility developed by [36] while the goodness of fit was tested using the Figure of Merit (FOM) of [37] given by:

$$FOM = \sum_{i} \frac{|Y_{Exper} - Y_{Fit}|}{A} \tag{7}$$

where Y_{Exper} is the experimental glow-curve, Y_{Fit} is the fitted glow-curve and A is the area of the fitted glow-curve. The FOM values obtained for the IRSL curves were of the order of 1.5–2.2%.

4. Results

The plots of Fig. 1 show examples for the three different modes of infrared stimulated luminescence signals, namely the conventional initial IRSL (Fig. 1a, b), MET-pIRIR (Fig. 1c, d), and pIRIR signals for two different initial stimulation temperatures, namely for 50 °C (Fig. 1e, f) and for 150 °C (Fig. 1g, h). Both not-normalized (Fig. 1a, c, e and g) and normalized curves (Fig. 1b, d, f and h) are presented. Normalization was performed over the maximum initial intensity, in order to monitor possible changes taking place in the shape of the various IRSL curves. Unless otherwise stated, hereafter the term MET-pIRIR, without any subscript, denotes the series of measurement starting from 25 up to 300 °C.

According to Fig. 1b, the normalized curves for the cases of conventional IRSL measurements coincide and have identical shape, which is independent of the stimulation temperature. The same is also indicated for the MET-pIRIR normalized curves presented in Fig. 1d. This behaviour is very similar to the previously studied isothermal TL curves in the same material as well as MgB_4O_7:Dy, Na [23,24] respectively, as well as to the IRSL curves of polymineral samples [25]. In these three previous studies, this behaviour of small changes taking place in the shape of the IRSL curves was interpreted as being indicative of the presence of tunnelling recombination processes. Similar experimental evidence was also reported for the case of Thermally Assisted OSL (TA-OSL) signal arising from very deep traps of Durango apatite [38].

The fact that a similar behaviour is found here for the MET-pIRIR signal provides experimental evidence for a tunnelling recombination process also being present in this type of signal. Fig. 1d shows that the normalized signals from the first IR stimulations at 50 and 75 °C are significantly different from the rest of the MET-pIRIR signals. This difference is most likely due to the presence of thermally unstable signals originating from shallow traps, being an experimental feature in very good agreement with the corresponding TR IRSL and TR-pIR IRSL curves presented by [19]. These authors also reported a large increase in the decay rate of TR-IRSL from 50 to 100 °C, and thereafter the change in the decay rate was reported to be very small and gradual. Similar results were also yielded for the other cases of pIRIR and MET-pIRIR series of measurements; nevertheless, only the results of the full MET-pIRIR series are presented, as these were considered as representatives.

A different behaviour is observed for the case of the normalized curves of $pIRIR_{50,Tb}$ signals in Fig. 1f; the subscript 50 indicates that the stimulation temperature of the initial IRSL is 50 °C. According to these data, it becomes clear that the shape of the normalized pIRIR signals changes with increasing stimulation temperature and consequently the corresponding normalized curves do not coincide. As the de-convolution analysis presented later in this paper will show, this change of shape could be partly attributed to the overlap of different tunnelling components, as well as to the differential contribution of each tunnelling component as the IRSL stimulation temperature is increased. A similar change in shape is also shown in Fig. 1h for the case of $pIRIR_{150,Tb}$ signal, which were measured at a stimulation temperature of 150 °C.

Applying a mathematical de-convolution to the data becomes mandatory in order to discriminate between the various components present in the signals. The effect of elevated temperature on the IRSL, MET-pIRIR and pIRIR curves is reflected on the values of the fitting parameters obtained during the de-convolution process. Analysis of all data in Fig. 1 shows that there are two tunnelling components, that have both been identified and discriminated, based on the analysis of both IRSL and pLM-IRSL modes. Fig. 2 presents a typical example on the de-convolution procedure. It is important to note that two tunnelling components were also found in recent studies of K-feldspar samples [26]. A fast component is the dominant one in these signals, while a second slower component is required in order to achieve good fitting.

In order to check the sensitivity and correctness of the results obtained by de-convolving the pLM curves, a reverse transformation from pLM-IRSL to CW-IRSL signals was also applied. This task was performed by carrying out an inverse conversion from the independent parameter "u" of the pLM curves, to the independent parameter "t" of the CW-IRSL signals. Yet, inverse transformation among the τ parameters needs extra mathematical study. On the other hand, as it can be seen in Fig. 2d, a stable correlation and an one-to-one correspondence was observed between the parameters $\tau(u)$ and $\tau(t)$ obtained at different stimulation temperatures. Using the constant obtained from Fig. 2d, a good agreement was found between all parameters obtained from both the original IRSL signals, and the transformed pLM IRSL of signals. Hereafter, only the parameters obtained according to the de-convolution of the CW-IRSL signals will be presented; nevertheless, the results obtained via the de-convolution of the pLM curves indicate similar trends.

Fig. 3a presents the behaviour of the integrated IRSL signal intensity versus stimulation temperature for the conventional IRSL signal measured at 50 °C. The intensity of the dominant IRSL component increases abruptly up to 75 °C, and then it stays almost independent of the stimulation temperature. On the contrary, the integrated intensity of the second component increases with the stimulation temperature until it reaches a maximum at a temperature of ~175 °C; above that stimulation temperature, the intensity of the second component starts decreasing. Fig. 3b shows similar behaviour of the MET-pIRIR signal, indicating a similar peak shaped behaviour for the integrated IRSL signal of both MET-pIRIR components, with the maximum intensity monitored at 200 °C. It is concluded that both the conventional IRSL and the MET-pIRIR signals yield similar behaviours, indicating independence or very mild dependence on the stimulation temperature. As it will be shown later in this paper, the temperature dependence of both components for the case of pIRIR signals is much more straightforward. This will be further discussed in the discussion section of this paper.

The plots of Fig. 4 present the dependence of the lifetime parameter $\tau(T)$ for the tunnelling process, obtained from the de-convolution analysis of both components of the conventional IRSL (shown in plot a), the MET-pIRIR signals (shown in plot b) and the pIRIR signals (shown in plots c and d). These figures indicate that the parameter τ for the first component is almost constant and independent of the stimulation temperature, for all three types of IR stimulation, with one

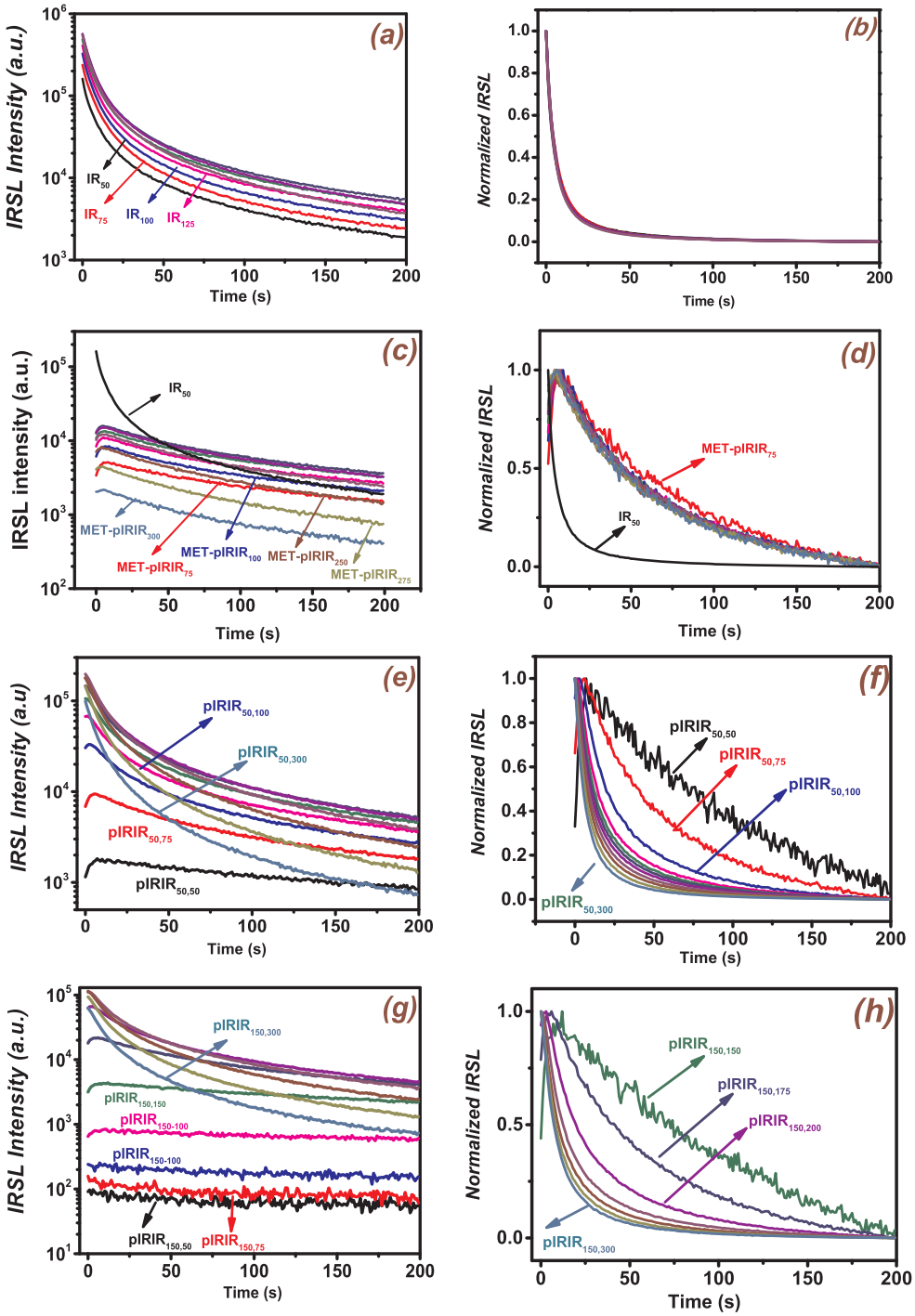

Fig. 1. Infrared stimulated luminescence behaviour of different IR modes; (a,b) conventional IRSL, (c,d) MET-pIRIR, (e,f) $pIRIR_{50,T_b}$ signals and (g,h) $pIRIR_{150,T_b}$ signals respectively. Luminescence signal shapes (a,c,e,g) and normalized signal shapes (b,d,f,h) of conventional, MET-pIRIR, $pIRIR_{50,T_b}$ and $pIRIR_{150,T_b}$ procedures, respectively. The subscripts 50 and 150 indicate that the stimulation temperature of the initial IRSL is 50 °C and 150 °C respectively.

exception noted for the initial stimulation temperatures (50–75 °C). For the case of the first component of the pIRIR signal, the behaviour is plotted at Fig. 4d, only for two initial stimulation temperatures, namely 50 and 75 °C; these temperatures were selected as being most meaningful. These figures show that the value of the lifetime parameter τ for the second tunnelling component increases linearly with the stimulation temperature.

All pIRIR fitting results are presented in Fig. 4c. Unfortunately, low statistics were present for the cases when the stimulation temperature of the pIRIR signal is lower than the stimulation temperature of the initial IRSL, namely within the temperature range 50–150 °C for pIRIR protocols. These low statistics resulted in large scattering in the fitting parameters, as it can be seen in Fig. 4c. Nevertheless, the signal statistics were gradually improved as the stimulation temperature reaches 175 °C and above. Once again, the most meaningful results are presented for the cases when the initial stimulation temperature is 50 or 75 °C. For those temperatures, the lifetime τ increases almost linearly with the stimulation temperature, while the density of acceptors ρ' does not change at the high stimulation temperatures. Assuming that the value of the dimensionless density of acceptors is large and independent of the stimulation temperature, the increase of the τ parameter provides a strong hint towards the fact that the second

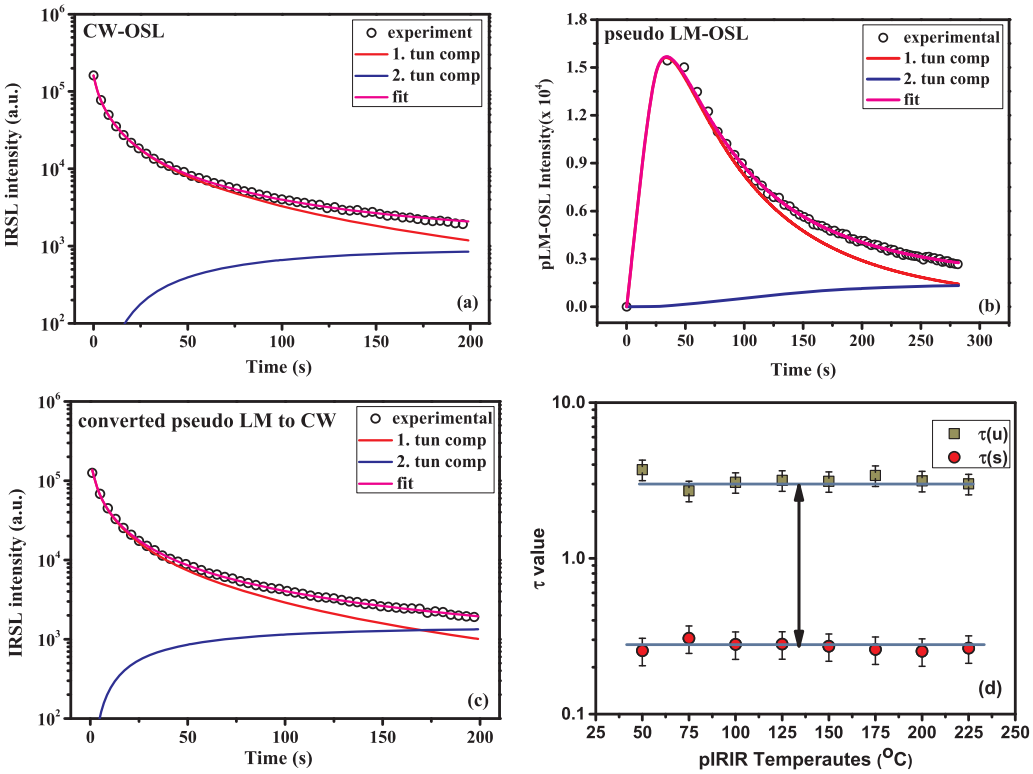

Fig. 2. An example of the signal analysis using tunnelling equations for: (a) CW-IRSL signal, (b) transformed pLM-IRSL signal, (c) Conversion of the pLM signal back to a CW-IRSL signal, in order to check the consistency of the method of analysis, (d) $\tau(u)$ - $\tau(t)$ correlation between the characteristic lifetimes of the pLM and CW-IRSL signals.

components of all three signals (IRSL, pIRIR, MET-pIRIR) indeed take advantage of more distant recombination centres as the stimulation temperature is increased.

In order to check the validity of the assumption that the value of the dimensionless density of recombination centres is stable, special emphasis is directed towards the experimental results for the ρ′ values obtained according to the de-convolution analysis of the corresponding signals. For each component of all aforementioned stimulation modes, these ρ′ values are independent on the stimulation temperature, yielding a corresponding distribution. In Fig. 5, a total of six histograms is presented. For the case of initial IRSL and MET-pIRIR, the distributions of both applied components are presented. However, for the case of pIRIR signals, only the distributions corresponding to the first component are plotted, and just for the cases of $pIRIR_{50,Tb}$ and $pIRIR_{150,Tb}$ signals. Each histogram is accompanied by the corresponding Gaussian distribution presented as solid line. In all cases, the values of the ρ′ parameter for the second component of the pIRIR signals were found similar to the values of the second component of the MET-pIRIR signals. The values of the ρ′ parameter indicate distribution centred around $7{\cdot}10^{-5}$, with quite wide and scattered histograms, and are not shown here. Table 1 presents a tabulated form of the fittings results regarding the Gaussian parameters for the distributions presented in Fig. 5.

Based on the plots of Fig. 5 and in conjunction to Table 1, the following conclusions can be reached:

1. The values of the ρ′ parameter for the first IRSL component is of the same order of magnitude with those reported by [39] despite the fact that these authors used only one component in their de-convolution analysis.
2. In both cases of IRSL and MET-pIRIR signals, the value of the ρ′ parameter of the second component is much smaller than the corresponding value for the first tunnelling component.
3. MET-pIRIR values of the ρ′ parameter are much smaller than those

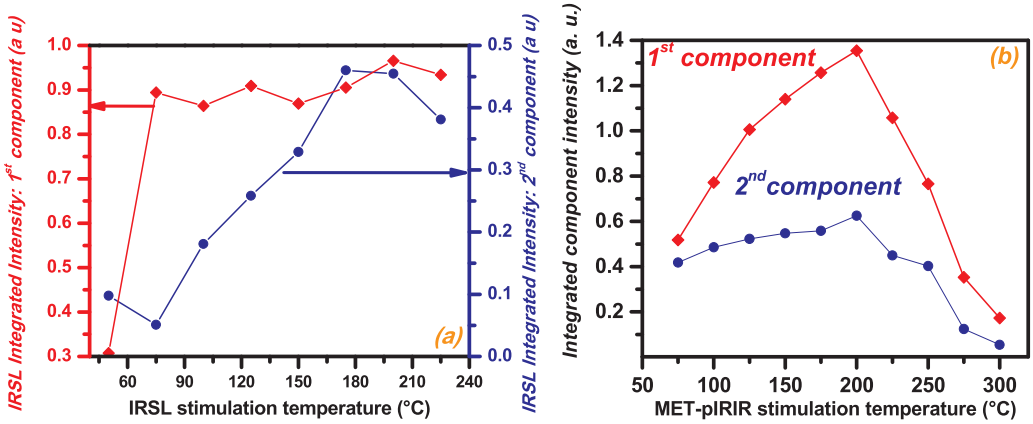

Fig. 3. Integrated IRSL intensity of both tunnelling components, as yielded by the de-convolution procedure, versus stimulation temperature for the case of the conventional IRSL signal (plot a) as well as the MET-pIRIR signal (plot b). For the latter case, the stimulation temperature corresponds to the temperature of the final stimulation step.

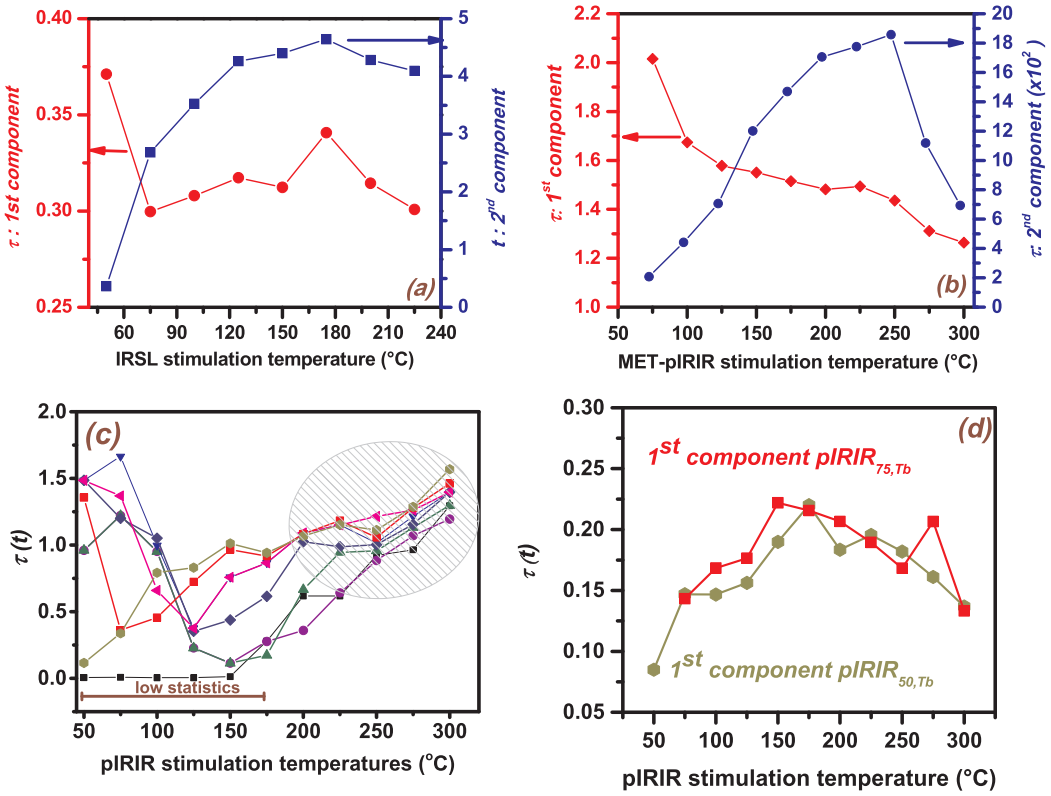

Fig. 4. Fitting results regarding the τ parameters plotted versus stimulation temperatures for the cases of (a) both components of conventional IRSL, (b) both components of MET-pIRIR and (c) only the second component of all pIRIR procedures; the dependence of the first component is plotted only for the cases of $pIRIR_{50,Tb}$ and $pIRIR_{75,Tb}$ at plot (d). For the latter case, the stimulation temperature corresponds to the temperature of the final stimulation step, while for the case of the $pIRIR_{50,Tb}$, the temperature corresponds to the second measurement.

obtained for the IRSL signals.

4. The Gaussian contributions obtained for both components of the conventional IRSL signals are quite narrow; however, the corresponding distributions for the cases of MET-pIRIR signals are much wider.
5. For the first component of the pIR IRSL signal, the values of the ρ′ parameter obtained by the de-convolution procedure are very close to both the IRSL of the first component, as well as to the values reported by [39]. The last plot in Fig. 5 shows clearly that as the stimulation temperature is increasing, the histogram for the ρ′ values shifts to lower values, while the corresponding distributions become wider.

Fig. 6 presents the dependence of the contribution of the second component of the IRSL signals of various stimulation modes, in terms of integrated signal, as obtained from the de-convolution procedure. It is worth emphasizing that the contribution of the second IRSL component could be considered stable and independent of the stimulation temperature for the cases of conventional IRSL and MET-pIRIR. Fig. 6 also shows that there is a sharp increase of this latter contribution at 75 °C, followed by a mild decrease and eventually a plateau for higher temperatures. However, in the case of pIRIR signals, the contribution of the second component is decreasing. Only the most meaningful cases are presented in Fig. 6, namely when the initial stimulation temperature is 50 or 75 °C. This de-convolution feature stands in excellent agreement with the change monitored in the shape of all pIRIR curves at different stimulation temperatures.

It should be emphasized that in the present study, all corresponding IRSL signals were measured after applying a test dose immediately without any preheating treatment. The use of a preheating was avoided in order to achieve good signal statistics, as these are crucial within any de-convolution analysis. The potential problem without applying a preheat before any IRSL measurements at elevated temperatures is that the measured IRSL and pIRIR signals may possibly be contaminated with thermal luminescence from thermally unstable traps [40]. Indeed, this signal contamination is monitored for the low stimulation temperatures, as Figs. 1, 3a and 4a indicate. The presence of this thermal luminescence contamination could be identified by the initial increasing part of the IRSL decay curves. However, as the stimulation temperatures increase further than 75 °C, at higher stimulation temperatures, as the material is heated in order to reach the specific stimulation temperature, this contribution becomes negligible. Moreover, the use of low heating rate while heatings at the selected temperature before IRSL is also important towards this direction.

5. Discussion

According to the results presented previously, one can safely conclude that both conventional as well as MET-pIRIR signals yield features that are independent on the stimulation temperature. The only signal entity that yields a full temperature dependence is the pIRIR signal; this dependence was observed not only for the parameters that characterise the decay of the pIRIR signal, but also for the corresponding integrated intensity. Previously [19,20], have also demonstrated the temperature dependence via the corresponding Arrhenius plots.

Fig. 7 presents the Arrhenius plots for several IRSL entities. Plot (a) deals with both components of the MET-pIRIR signals as well as the first component of the conventional IRSL signal. At this point it is useful to remind that according to Fig. 3, there is not any temperature dependence for the intensity of the second component of the IRSL signal. The corresponding analysis of the data indicates thermal activation energies of 0.03 ± 0.005 eV for the 2nd MET-pIRIR component, 0.05 ± 0.011 eV for the 1st MET-pIRIR component and 0.10 ± 0.015 eV for the case of the 1st component of the conventional IRSL. All these three values are consistent with previously reported activation energy values of phonon modes, and are in good agreement

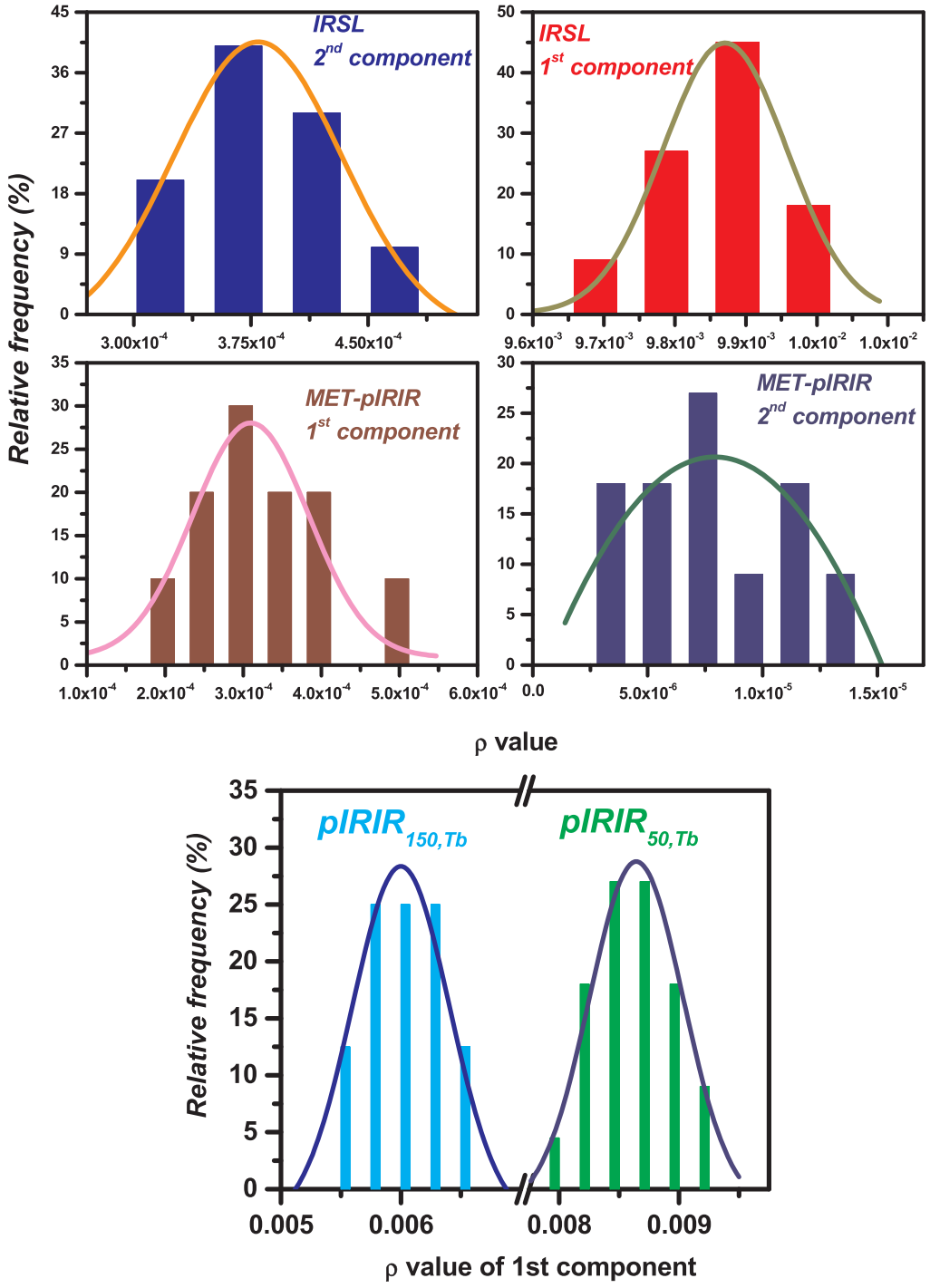

Fig. 5. The histograms for the dimensionless parameter ρ of both components for the cases of IRSL (upper plots) as well as MET-pIRIR signals (middle plots). Lower plots present the histogram of the same parameter for the first component of both $pIRIR_{50,Tb}$ and $pIRIR_{150,Tb}$ signals. The corresponding Gaussian distribution presented as solid line accompanies each histogram.

Table 1
Gaussian fitting results for the distributions presented in Fig. 5.

A/A	Signal	Component	Centroid	σ
1	IRSL	First	$9.87 \cdot 10^{-3}$	$8.51 \cdot 10^{-5}$
2	IRSL	Second	$3.85 \cdot 10^{-4}$	$5.38 \cdot 10^{-5}$
3	MET-pIRIR	First	$3.71 \cdot 10^{-3}$	$2.51 \cdot 10^{-4}$
4	MET-pIRIR	Second	$9.85 \cdot 10^{-5}$	$4.38 \cdot 10^{-5}$
5	$pIRIR_{50,Tb}$	First	$8.64 \cdot 10^{-3}$	$4.51 \cdot 10^{-4}$
6	$pIRIR_{50,Tb}$	First	$6.00 \cdot 10^{-3}$	$6.74 \cdot 10^{-4}$

with measured phonon mode energies for strong lattice vibrations in feldspars [41,42].

On the contrary, thermal assistance effects are more prominent in the case of pIRIR signals. According to Fig. 7b, both components of $pIRIR_{50,Tb}$ signals yield strong thermal assistance, with thermal activation energies of 0.33 ± 0.032 eV for the 1st component as well 0.17 ± 0.012 eV for the 2nd component. Besides the thermal activation energy of 0.33 eV obtained for the 1st pIRIR component, the rest of the thermal activation energy values stand in good agreement with those reported by [19].

According to [43], the IRSL trap lies 2.5 eV below the conduction

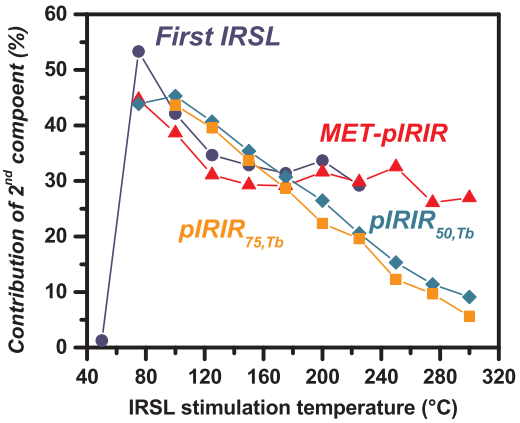

Fig. 6. The contribution of the second component to the IRSL signal, in terms of the integrated signal intensity, for the cases of conventional IRSL, MET-pIRIR, $pIRIR_{50,Tb}$ and $pIRIR_{75,Tb}$ signals.

band, while [41] suggested that this energy does not exceed 2 eV. As infrared stimulation provides around 1.45 eV, the excitation is into the sub-conduction band; therefore, thermal activation energies correspond to the additional amount of thermal energy offered by heating. According to the thermal activation energies listed above, thermal assistance does not place charge in the conduction band, but most likely results in thermal diffusion within the lattice and within the potential recombination volume. The trapped electrons are placed at the excited state of the trap, while from there electrons can recombine by tunnelling and/or via band tail transport. The fact that a large number of components after IRSL and MET-pIRIR excitation is characterised by similar thermal activation energy (0.03–0.17 eV) implies the presence of phonon assisted tunnelling, suggesting that a significant proportion of the excited electrons thermalize until they finally occupy an equilibrium energy distribution. Even the thermal activation energy for the second pIRIR component, which was calculated to be 0.17 ± 0.012 eV, corresponds to a lattice phonon mode of 0.05 eV.

According to the de-convolution results, it is concluded that the first, fast tunnelling component describes the tunnelling recombination from the excited state. This result could be concluded based on: (a) the lowest possible lifetime τ, since the lifetime of the tunnelling recombination from the excited state is expected to occur within the shortest duration, (b) Fig. 4a, b and d; besides the initial change of the lifetime τ in the temperature region 50–100 °C for the initial IRSL, the lifetime is independent of the stimulation temperature. This feature provides a strong argument towards a tunnelling mechanism. The second, slower component originates from transport through the band tail states. Two different types of recombination from the band tails are possible, namely caused by a combination of phonon assisted diffusion and tunnelling from the deepest disconnected band tail states. As the temperature is further increased for the case of pIRIR signal, the contribution of the second component decreases. Therefore, at relatively low stimulation temperatures, the high energy, high mobility band tail states contribute to the slow IRSL signal. As the stimulation temperature is further increased, the slow component includes higher contributions from the low energy, low mobility band tail states.

Based on this scenario, the strong increase in both the decay rate as well the integrated intensity of the fast pIRIR signal with stimulation temperatures, could also be attributed to thermally enhanced transitions from the excited state to the band tail states, which result in an overall decrease in the residence time of the excited state. Moreover, it becomes obvious from the corresponding Arrhenius plots that the pIRIR mode gets the electrons even closer to the conduction band. Nevertheless, with reference to the fast pIRIR component, one could have expected that a tunnelling recombination process would have not indicated intense thermal assistance. By increasing the temperature, a greater fraction of electrons is placed in the excited state, while a greater proportion of these electrons make a thermal escape from this excited state into the band tails. It becomes apparent that the fast pIRIR signal mainly originates from a longer transport within the band tails. Moreover, this behaviour is also similar to that reported by [39] who have indicated that an increase at the stimulation temperature of the conventional IRSL influences only the intensity, but not the decay rate. This observation clearly suggests that the IRSL decay rate does not reflect the de-trapping rate, but instead the recombination probability; the higher the stimulation temperature, the greater the recombination probability. As the stimulation temperature increases, electrons reach higher energies and an exponential increase in the density of states is expected, resulting in an efficient sub E_c transport, especially for the fast component.

The infrared stimulation places electrons in the excited state. Then, because of the elevated temperatures at which IRSL measurements occur, thermally assisted diffusion takes place from the excited state to the band tails. The higher the thermal assistance, more electrons reach the lower energy states as well as the disconnected band tail states. According to Fig. 3b, the integrated intensity of the fast MET-pIRIR component yields a maximum at the temperature of 175 °C; after the temperature of 175 °C, a monotonic decrease is yielded. This temperature represents the threshold at which the dominance of the two band tail emptying mechanisms changes. Before 175 °C thermal diffusion is dominant, while above 175 °C the tunnelling from the disconnected band tail states of extremely low charge mobility, becomes dominant. Therefore, in the framework of the MET-pIRIR protocol, at high stimulation temperatures the second component is dominated by the tunnelling from the disconnected band tails; this is the reason why the

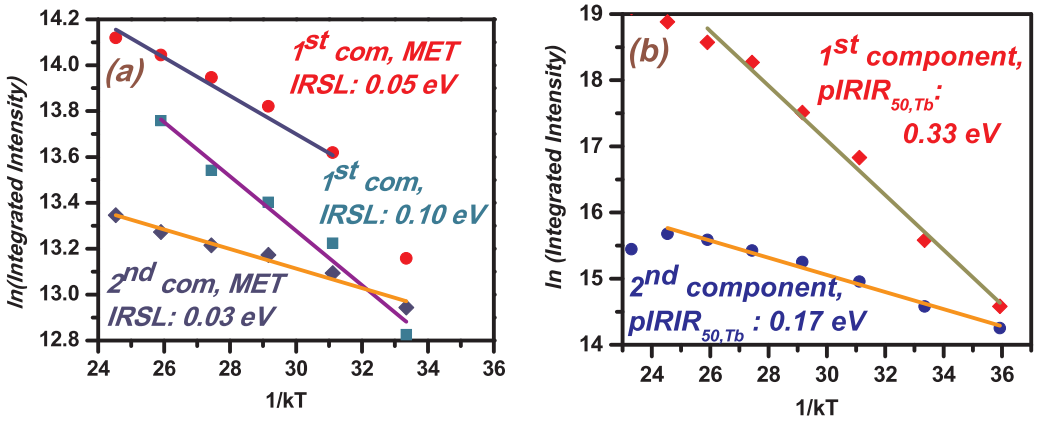

Fig. 7. Arrhenius plots for various components of conventional and MET-pIRIR signals (plot a) as well as for the $pIRIR_{50,Tb}$ signals (plot b). Linear regressions along with the corresponding slopes are also presented.

signal does not yield temperature dependence. It should be highlighted that recombination can also occur via tunnelling from the deeper band tail states within the band gap, even at room temperature (RT). Nevertheless, at RT the contribution is too low and the decay too slow.

The first IR bleaching (conventional IRSL) consumes the proximal pairs by recombination from around the excited state of the trap. A subsequent IRSL measurement at elevated temperature is able to access a greater volume of the crystal through the high energy band tail states, thus being able to access distant holes. The change in the integrated IRSL signal intensity of the fast component with IR stimulation temperature, as presented at Figs. 3 and 7, suggests an increased partitioning from the excited state to the higher energy band tail states. According to [19], it is expected from the Boltzmann's distribution that a proportion of these electrons will eventually completely thermalize and come to occupy the deep, disconnected, band tail states. These are the electrons that are stimulated finally within the framework of MET-pIRIR measurements at elevated temperatures. The nearest holes are preferentially consumed by the tunnelling via the excited state. As the IR stimulation proceeds further, it sweeps out increasingly distant pairs. The fast component arises from more localized recombination than the slow component. The ground state tunnelling is the most localized recombination; band tail recombination follows while conduction band recombination accesses, in principle, the entire crystal.

Based on this rationale, it becomes evident that the only procedure that can access a greater volume of the crystal, resulting in a decrease of the available number of centres, is the pIRIR measurement. This is the reason why, the value of the τ parameter for the second component starts to increase, as the first component travels more within the band tails, sweeping out increasingly distant pairs. According to the initial model by [21], the dimensionless density parameter ρ' should remain constant, and this is in agreement with the experimental data in this study, where a stable value of the dimensionless parameter ρ' is found throughout the entire range of stimulation temperatures. This stability of ρ' is found for all three cases of IRSL signals (conventional IRSL, pIRIR and MET-pIRIR).

An increase of the τ parameter, in conjunction with the practically constant dimensionless parameter ρ' indicates that the recombination process requires gradually more time due to the fact that electrons recombine with more distant holes at higher stimulation temperatures. A second IRSL measurement at elevated temperature is able to access a greater volume of the crystal through the high energy band tail states, and thus is able to access more distant holes. This feature is clearly highlighted by the thermal assistance features of the fast component.

The present work can give some important insights to the physical meaning of the dimensionless parameter ρ'. According to the distributions of Fig. 5, it is suggested that the value of this parameter could be related to the energy and mobility of the band tail states; the lower these values get, the more disconnected these band tails are.

Fig. 8 presents the results on the residual TL (rTL) glow curves that were measured throughout the present study. Plot (a) presents the rTL glow curves after all measurements of $pIRIR_{50,Tb}$ sequence. A general observation is that IR stimulation does not influence all electron traps responsible for the TL signal in the same manner. The influence of the IR stimulation seems to be stronger at the low temperature part of the TL glow curve, and decreases gradually as the temperature increases along the TL glow-curve. This behaviour is characteristic of a localized transition and has been reported recently by both [44] as well as [28]. Moreover, there is a part of the high-temperature TL glow curve which remains unaffected by all IRSL modes, no matter how high the stimulation temperature gets. The temperature range of this unaffected part of the TL glow curve ranges between 375 and 500 °C. As one increases the stimulation temperature, one expects that nearby donor-acceptor pairs will recombine first, while pairs that are more distant will remain unaffected. This in turn will lead to a reduction of the luminescence signal in the low temperature side of the TL glow curves, since it is reasonable to assume that this part of the TL glow curve corresponds to shorter pair distances. This effect of thermal or optical stimulation on the low temperature side of the TL glow curves was

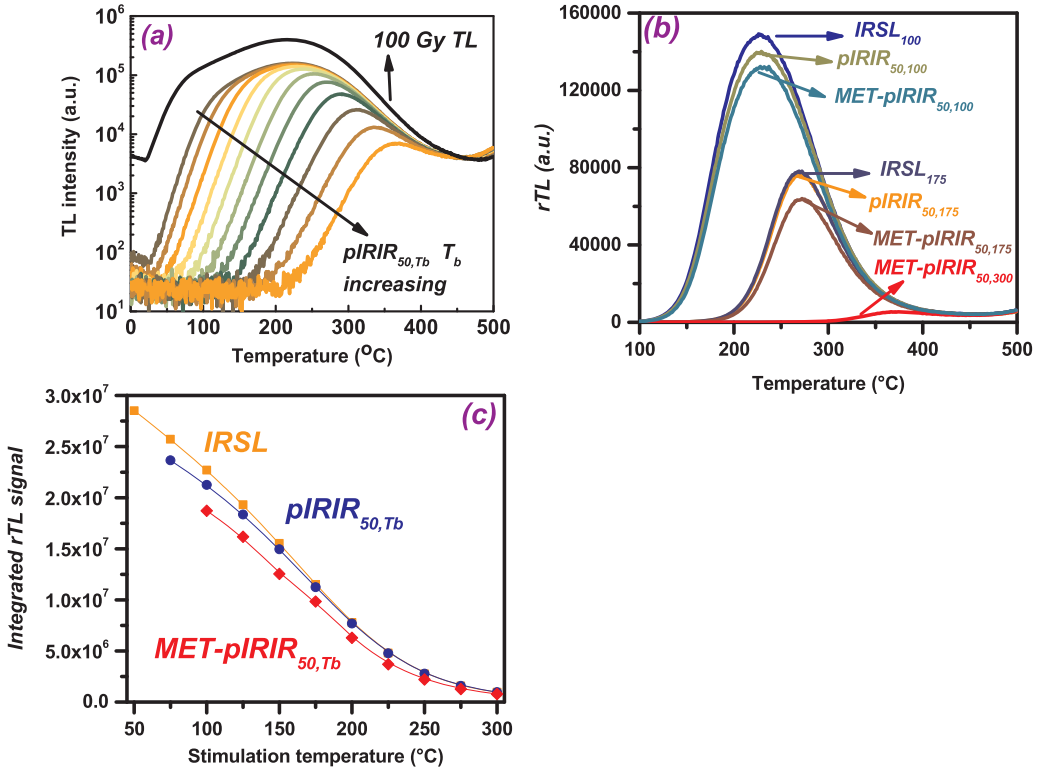

Fig. 8. Plot (a) presents the rTL glow curves after the $pIRIR_{50,Tb}$ of all temperatures, along with the prompt TL corresponding to 100 Gy dose without any IRSL measurement. Plot (b) presents rTL curves for a selection of IRSL modes and a selection of temperatures. Finally, plot (c) presents the integrated rTL intensity after IRSL (squares), $pIRIR_{50,Tb}$ (dots) and MET-pIRIR (diamonds).

previously demonstrated by [19] (their Fig. 9), which showed that the high temperature side of the TL glow curve remains unaffected. Plot (b) presents a selection of rTL glow curves for a selection of modes and stimulation temperatures, while plot (c) presents the integrated rTL intensity for the cases of IRSL (squares), $pIRIR_{50,Tb}$ (dots) and MET-pIRIR (diamonds). Since IRSL is a single step measurement procedure, $pIRIR_{50,Tb}$ is a double step measurement procedure and MET-pIRIR is a multi step measurement procedure, the integrated rTL intensity is plotted versus the stimulation temperature of the last step/measurement of the corresponding modes. According to these latter two plots, it becomes obvious that in the temperature region ranging between RT and 125 °C, the integrated rTL signals differ substantially, with the residual TL being higher for the case of the IRSL measurement, while the rTL of the MET-pIRIR measurements is the lower. This latter result could be easily explained, since the latter mode involves multi step IRSL measurements at elevated temperatures. As the stimulation temperature of the last IRSL further increases, the integrated rTL signals of IRSL and $pIRIR_{50,Tb}$ coincide; however, still the integrated rTL signals of MET-pIRIR measurements are still lower. Finally, at the temperatures of 275 and 300 °C, all three stimulation modes at high temperatures give the same integrated rTL intensity. As this latter intensity corresponds to the signal that was not stimulated by IRSL, it is safe to conclude that from stimulation temperatures above 150 °C, IRSL and $pIRIR_{50,Tb}$ stimulate exactly the same signal, in terms of quantitative intensity. However, from a qualitative point of view, these two stimulation modes result in different recombination pathways, depending on the thermal activation energy. This model assumes that band tail states are characterised by a variety of well depths, widths and separations.

Within the framework of the existing models, both results and interpretation of the present data seem reasonable. Nevertheless, precisely because interpretation is based on consensus and concepts, rather than precise mechanisms with unequivocal evidence, further work is required to add in some additional types of information. The presence of two components could signify the presence of two emission bands. Therefore, spectral response studies will possibly be of great importance, as it is likely that the different emission spectra could exist in each stimulation case, not just for different feldspar types only, but also for different processing treatments of the same material.

6. Conclusion

In this paper, a set of promising results was put forward in the framework of a comprehensive research project. While some of the results supported former research, other results are introduced for the first time in the literature. Various types of infrared stimulated luminescence signals (from a microcline K-feldspar) were investigated, and the effect of stimulation temperature on the IRSL, MET-pIRIR and pIRIR curves was presented in a quantitative manner.

Experimental IRSL curves were de-convolved successfully using the tunnelling Eqs. (1)–(3), for both CW and pLM-OSL curves. Results are in good agreement with recent research reported by [19] and [44]. According to the residual TL (rTL) glow curves, that were measured throughout the present study, IR stimulation does not influence all electron traps responsible for the TL signal and the influence of the IR stimulation is stronger at the low temperatures.

Within the framework of the existing models, both results and interpretation of the present data seem reasonable. We believe that the results presented here improve the understanding of the community on the origin of luminescence signals from feldspars. Further work is required (a) to apply similar protocols to various types of feldspars, (b) to apply other techniques such as electron spin resonance (ESR) and time resolved optically stimulated luminescence, (c) to investigate whether the presence of two IR components could signify the presence of two emission bands and finally (d) dependence of spectral response on the type of the measurements.

Acknowledgements

The corresponding author (E.Ş.) wants to thank Ankara University Rectorate/Senate for giving him permission to perform post doctorate research abroad and all staff of Nuclear Physics Laboratory, Physics Department, Aristotle University of Thessaloniki for hosting and for their support.

References

[1] E. Şahiner, Physics Engineering Department (Ph.D. thesis), Ankara University, Turkey, 2015.
[2] E. Şahiner, N. Meriç, S.G. Polymeris, Nucl. Instrum. Methods B 392C (2017) 21–30.
[3] A.G. Wintle, Nature (1973) 143–144.
[4] M.J. Aitken, Thermoluminescence Dating, Acedemic Press, London, 1985, p. 359.
[5] D.J. Huntley, M. Lamothe, Can. J. Earth Sci. 38 (7) (2001) 1093–1106.
[6] M. Auclair, M. Lamothe, S. Huot, Radiat. Meas. 37 (4) (2003) 487–492.
[7] B. Li, Radiat. Meas. 45 (2010) 757–763.
[8] K.J. Thomsen, A.S. Murray, M. Jain, L. Bøtter-Jensen, Radiat. Meas. 43 (9) (2008) 1474–1486.
[9] B. Li, S.H. Li, Quat. Geochronol. 10 (2012) 24–31.
[10] J.P. Buylaert, A.S. Murray, K.J. Thomsen, M. Jain, Radiat. Meas. 44 (5) (2009) 560–565.
[11] J.P. Buylaert, M. Jain, A.S. Murray, K.J. Thomsen, C. Thiel, R. Sohbati, Boreas 41 (3) (2012) 435–451.
[12] C. Thiel, J.P. Buylaert, A. Murray, B. Terhorst, I. Hofer, S. Tsukamoto, M. Frechen, Quat. Intern. 234 (1) (2011) 23–31.
[13] T. Reimann, S. Tsukamoto, M. Naumann, M. Frechen, Quat. Geochronol. 6 (2) (2011) 207–222.
[14] X. Fu, B. Li, S.H. Li, Quat. Geochronol. 10 (2012) 8–15.
[15] B. Li, Z. Jacobs, R.G. Roberts, S.H. Li, Geochronometria 41 (3) (2014) 178–201.
[16] B. Li, R.G. Roberts, Z. Jacobs, S.H. Li, Quat. Geochronol. 20 (2014) 51–64.
[17] Y. Chen, S.H. Li, B. Li, Q. Hao, J. Sun, Quat. Geochronol. 30 (2015) 207–212.
[18] Z. Gong, B. Li, S.H. Li, J. Lumin. 159 (2015) 238–245.
[19] M. Jain, C. Ankjærgaard, Radiat. Meas. 46 (3) (2011) 292–309.
[20] M. Jain, R. Sohbati, B. Guralnik, A.S. Murray, M. Kook, T. Lapp, A.K. Prasad, K.J. Thomsen, J.P. Buylaert, Radiat. Meas. 81 (2015) 242–250.
[21] M. Jain, B. Guralnik, M.T. Andersen, J. Phys. Condens. Matter 24 (38) (2012) 385–402.
[22] V. Pagonis, G. Polymeris, G. Kitis, Radiat. Meas. 82 (2015) 93–101.
[23] K. Sfampa, G.S. Polymeris, N.C. Tsirliganis, V. Pagonis, G. Kitis, Nucl. Instrum. Methods B 320 (2014) 57–63.
[24] G. Kitis, G.S. Polymeris, I.K. Sfampa, M. Prokic, N. Meric, V. Pagonis, Radiat. Meas. 84 (2016) 15–25.
[25] E. Şahiner, N. Meriç, G.S. Polymeris, Radiat. Meas. 68 (2014) 14–22.
[26] G. Kitis, V. Pagonis, J. Lumin. 137 (2013) 109–115.
[27] G.S. Polymeris, E. Theodosoglou, G. Kitis, N.C. Tsirliganis, A. Koroneos, K.M. Paraskevopoulos, Medit. Arch. Archaeom. 13 (3) (2013) 155–161.
[28] K. Sfampa, G.S. Polymeris, V. Pagonis, E. Theodosoglou, N.C. Tsirliganis, G. Kitis, Nucl. Instrum. Methods B 359 (2015) 89–98.
[29] G. Kitis, G.S. Polymeris, E. Sahiner, N. Meric, V. Pagonis, J. Lumin. 176 (2016) 32–39.
[30] L. Bøtter-Jensen, G.A.T. Duller, A.S. Murray, D. Banerjee, Radia. Prot. Dosim. 84 (1999) 335–340.
[31] L. Bøtter-Jensen, V. Mejdahl, A.S. Murray, Quat. Sci. Rev. 18 (2) (1999) 303–309.
[32] G. Kitis, G.S. Polymeris, N.G. Kiyak, Nucl. Instrum. Methods B 359 (2015) 60–63.
[33] I.K. Bailiff, N.R.J. Poolton, Nucl. Tracks Radiat. Meas. 18 (1991) 111–118.
[34] G. Kitis, G.S. Polymeris, N.G. Kiyak, V. Pagonis, Geochronometria 38 (3) (2011) 209–216.
[35] E. Bulur, Radiat. Meas. 32 (2) (2000) 141–145.
[36] D. Afouxenidis, G.S. Polymeris, N.C. Tsirliganis, G. Kitis, Radiat. Prot. Dosim. 149 (3) (2012) 363–370.
[37] H.G. Balian, N.W. Eddy, Nucl. Instrum. Methods A 145 (2) (1977) 389–395.
[38] G. Kitis, G.S. Polymeris, V. Pagonis, N.C. Tsirliganis, Radiat. Meas. 49 (2013) 73–81.
[39] V. Pagonis, M. Jain, K.J. Thomsen, A.S. Murray, J. Lumin. 153 (2014) 96–103.
[40] B. Guralnik, B. Li, M. Jain, R. Chen, R.B. Paris, A.S. Murray, S.H. Li, V. Pagonis, P.G. Valla, F. Herman, Radiat. Meas. 81 (2015) 224–231.
[41] N.R.J. Poolton, J. Wallinga, A.S. Murray, E. Bulur, L. Bøtter-Jensen, Phys. Chem. Miner. 29 (2002) 210–216.
[42] N.R.J. Poolton, K.B. Ozanyan, J. Wallinga, A.S. Murray, L. Bøtter-Jensen, Phys. Chem. Miner. 29 (2002) 217–225.
[43] M.R. Baril, D.J. Huntley, J. Phys. Condens. Matter 15 (2003) 8011–8027.
[44] V. Pagonis, P. Morthekai, G. Kitis, Geochronometria 41 (2014) 168.